Gradient Based Optimization of Chaotic Panel Flutter

Bret K. Stanford*

NASA Langley Research Center, Hampton, VA, 23681

This work considers the gradient-based optimization of an aeroelastic panel structure undergoing chaotic vibrations. A previously-presented adaptive time-marching scheme is used to stabilize the design sensitivities which would normally grow unbounded in time, owing to intermittent unstable eigenvalues of the Jacobian. The design optimization entails forcing the root mean square (RMS) of the panel vibration to some specified value, in a way that minimizes the deviation of the structural thickness variables from their uniform baseline values. Depending on the location of the RMS constraint, the output physics may be chaotic, limit cycle oscillations, or statically buckled.

I. Introduction

A thin panel structure subjected to supersonic flow over its upper surface, as well as compressive in-plane loading (from, for example, thermal effects), can experience a range of dynamical outputs depending on the quantitative combination of those two inputs. The strong stabilizing geometrical nonlinearities of the panel structure can quench instabilities from aeroelastic flutter, leading to limit cycle oscillations (LCOs). If the in-plane loading is far enough beyond the buckling point, the panel dynamics may transition from an LCO to a chaotic output.[1] This paper is interested in computing the analytical derivative of some time-averaged quantity of interest (for example the root mean square, RMS, of the chaotic response) with respect to parametric inputs: the panel's shape, structural make-up, flow conditions, etc. These sensitivities can then be utilized in an optimization scheme, where the chaotic RMS response is introduced as a design constraint.

The well-known challenge to computing analytical sensitivities of chaotic systems is that the Jacobian, $\boldsymbol{J}$, of the nonlinear system will contain unstable eigenvalues at certain instances in time. This does not pose a problem for the forward analysis of the chaotic motion itself, as the structural nonlinearities will arrest unbounded motions. The linearized systems used to compute design sensitivities, conversely, become unbounded in time, and therefore do not provide useful results. Schemes developed to compute chaotic sensitivities include boundary value least-squares shadowing (LSS) schemes,[2,3] data-driven approaches,[4] real-time reduced order modeling,[5] and stabilized time marching schemes.[6,7]

The goals of this work are to utilize the stabilized scheme of Refs. 6 and 7 to explore the chaotic sensitivities of a two-dimensional panel structure (beyond the one-dimensional results shown in Ref. 7), and, as a more substantial extension, to utilize these sensitivities in a design optimization exercise. It is desired to find the smallest deviation in the structural thickness distribution (from the baseline, uniform, distribution) which will set the RMS of the output to some specified value.

II. Formulation

The panel physics are modeled with nonlinear shell finite elements for the structure, and piston theory for the supersonic aerodynamics. These equations of motion, and the extension into finite element solutions, are well known (see Ref. 8), and will not be repeated here. The final equations of motion are solved as:

$$\boldsymbol{M} \cdot \dot{\boldsymbol{x}} = \boldsymbol{R}(\boldsymbol{x}, \alpha) \tag{1}$$

where $\boldsymbol{M}$ is a mass matrix, $\boldsymbol{R}$ is a nonlinear residual, $\boldsymbol{x}$ is the solution vector (three displacements and rotations at each finite element node, as well the corresponding time derivatives), and α is an input parameter.

*Research Aerospace Engineer, Aeroelasticity Branch, bret.k.stanford@nasa.gov, AIAA Associate Fellow.

For a square, simply-supported panel (Fig. 1), with equal in-plane compressive tractions in both the chordwise and spanwise directions, the aeroelastic behavior is shown in Fig. 2, where λ is a dynamic pressure parameter, R is the in-plane loading parameter (R_{cr}, the buckling value, is $2 \cdot \pi^2$), and the ratio of μ (mass ratio) to M (Mach) is 0.1. Definitions for each nondimensional parameter can be found in Ref. 1, among others. Eq. 1 is solved on a 32×32 mesh, with symmetry assumed in the spanwise direction. The plot in Fig. 2 generally agrees with Ref. 8: at a R/R_{cr} value of 3, chaotic motions are obtained when λ is increased above 215, and then transitions to LCO when λ increases above 325. Time history plots on the right of Fig. 2 shows the thickness-normalized vertical displacement along the panel centerline, at the three-quarters chord location.

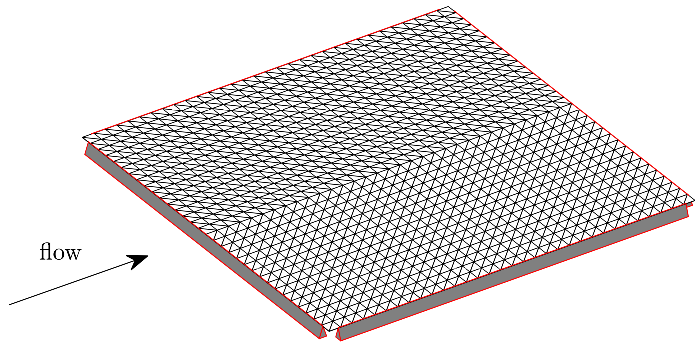

Figure 1: Simply-supported panel.

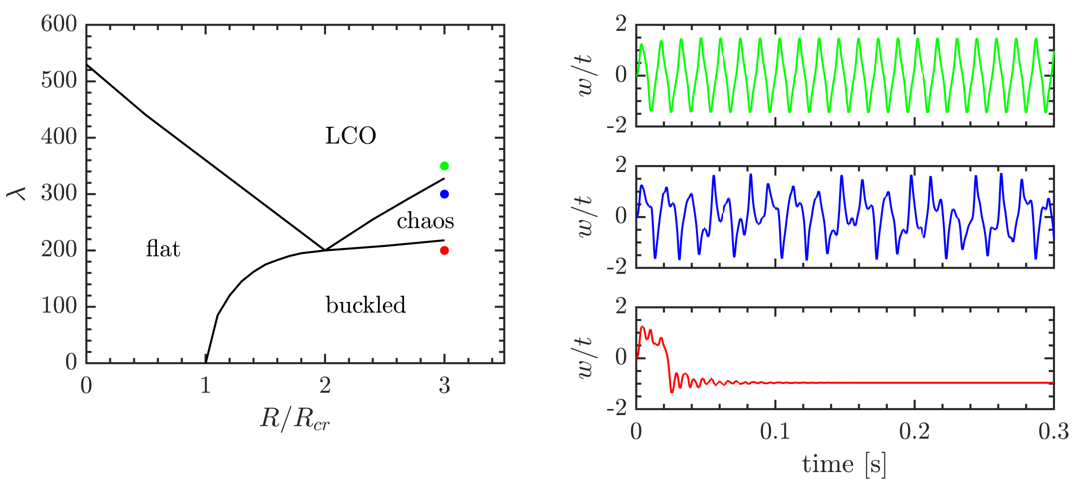

Figure 2: Panel stability boundaries (left), and sample time histories (right) at $R/R_{cr} = 3$, $\lambda = 200$ (static), $\lambda = 300$ (chaos), and $\lambda = 350$ (LCO).

Generalizing the output of interest as f (which may be the structural displacement, or some other metric), it is desired to compute a time-averaged value of this quantity, such as RMS:

$$F(\alpha) = \lim_{T\to\infty} \left[\frac{1}{T} \int_0^T f(\boldsymbol{x}, \alpha) \cdot dt \right] \tag{2}$$

The derivative of F with respect to α is given by:

$$F_\alpha = \lim_{T\to\infty} \left[\frac{1}{T} \int_0^T \left(f_\alpha + f_{\boldsymbol{x}}^T \cdot \boldsymbol{x}_\alpha \right) \cdot dt \right] \tag{3}$$

Using the direct method, $\boldsymbol{x}_\alpha$ can be computed by differentiating Eq. 1:

$$\boldsymbol{M} \cdot \dot{\boldsymbol{x}}_\alpha = \boldsymbol{J} \cdot \boldsymbol{x}_\alpha + \boldsymbol{R}_\alpha - \boldsymbol{M}_\alpha \cdot \dot{\boldsymbol{x}} \tag{4}$$

where the Jacobian $\boldsymbol{J} = \partial \boldsymbol{R}/\partial \boldsymbol{x}$. The Jacobian will have unstable eigenvalues for some portions of a chaotic response, rendering the time integration of Eq. 4 unstable, and the resulting F_α useless. Despite this, and as will be seen below, the chaotic panel response does contain clean and stable sensitivities. The RMS of the panel deformation (F) displays a strong convergence as T approaches ∞, and finite changes in α leads to coherent and consistent changes in F, for many definitions of α.

The time-stabilized scheme of Refs. 6 and 7 will be used to compute F_α, and will be briefly summarized here for completeness. Only the direct scheme is summarized; though the optimization results below necessarily use an adjoint scheme (as it is desired to compute derivatives with respect to a large vector of design parameters), this is a straightforward extension of the direct method, and the derivation can be found in the previous references. Using a variational analysis between consecutive time steps t_n and t_{n+1}, Eq. 4 can be written as:[6]

$$\left(\boldsymbol{M} - \boldsymbol{J}^{int}\right) \cdot \boldsymbol{x}_\alpha^{n+1} = \boldsymbol{M} \cdot \boldsymbol{x}_\alpha^{n} + \boldsymbol{F}^{int} \tag{5}$$

$$\boldsymbol{J}^{int} = \int_{t_n}^{t_{n+1}} \boldsymbol{J} \cdot dt \tag{6}$$

$$\boldsymbol{F}^{int} = \int_{t_n}^{t_{n+1}} \left(\boldsymbol{R}_\alpha - \boldsymbol{M}_\alpha \cdot \dot{\boldsymbol{x}}\right) \cdot dt \tag{7}$$

Eq. 5 is the recursive backwards-Euler update scheme, and will give an identical result to a numerically-integrated Eq. 4, as long as the Newmark parameters are set in Eq. 4 to those needed for a backwards-Euler method.

In order to maintain stability of Eq. 5, this equation is adaptively updated in time. The chaotic forward analysis Eq. 1 is updated at every time step, and the integrals of Eqs. 6 and 7 are accumulated until the matrix $\left(\boldsymbol{M} - \boldsymbol{J}^{int}\right)^{-1} \cdot \boldsymbol{M}$ meets some stability criterion. Once this is met, Eq. 5 is solved, the two integrals are set back to 0, and the process repeats. For the first 10 times steps, for example, the forward solution $\boldsymbol{x}$ will exist at every time step, but the derivative $\boldsymbol{x}_\alpha$ will only exist at time steps 0 (the initial condition), 6 and 10, assuming that $\left(\boldsymbol{M} - \boldsymbol{J}^{int}\right)^{-1} \cdot \boldsymbol{M}$ becomes stable at time step 6, and then again at time step 10.

In this work, the stability criterion is met when the largest eigenvalue of $\left(\boldsymbol{M} - \boldsymbol{J}^{int}\right)^{-1} \cdot \boldsymbol{M}$ is less than some value a. The value of a would nominally be set to 1, but smaller values can introduce more damping and stability into the analysis, by forcing less-frequent updating (i.e., larger adaptive time steps).

III. Results

A. Sensitivity Computations

First, sensitivities of the RMS response (of the vertical deflection at the three-quarters chord location along the centerline) with respect to the dynamic pressure parameter λ are demonstrated. Results are shown in Fig. 3 for R/R_{cr} set to 10 and λ set to 600. These results are integrated through 10 seconds, in order for the time-averaged quantity (RMS, shown in the center plot) to properly converge, though only the first 0.5 seconds are shown for ease of presentation. For the derivative of the final RMS value (at T=10) with respect to λ, the unstabillized result of Eq. 4 is unbounded, while the stabilized result (normalized by thickness-squared) of Eq. 5 converges near a value of 0.00186.

The time stabilization procedure is further highlighted in Fig. 4, which shows the first 500 time steps of Fig. 3, and a limiting a value of 0.8. The largest eigenvalue of $\left(\boldsymbol{M} - \boldsymbol{J}^{int}\right)^{-1} \cdot \boldsymbol{M}$ is shown on the upper plot, and 30 time steps elapse before this eigenvalue drops below 0.8. Before time step 30, and at later steps as well, the eigenvalue sporadically becomes larger than 10. At time step 30, Eq. 5 is solved, the two integrals in Eqs. 6 and 7 are set back to 0, and the process repeats, again updating at time step 45.

A verification of the computed sensitivities is shown in Fig. 5, for a range of λ values between 400 and 700. Each data point on these plots represents the statistical average of 100 separate simulations. As noted above, there is a strong and coherent trend in RMS with changes in λ, although small variations in RMS

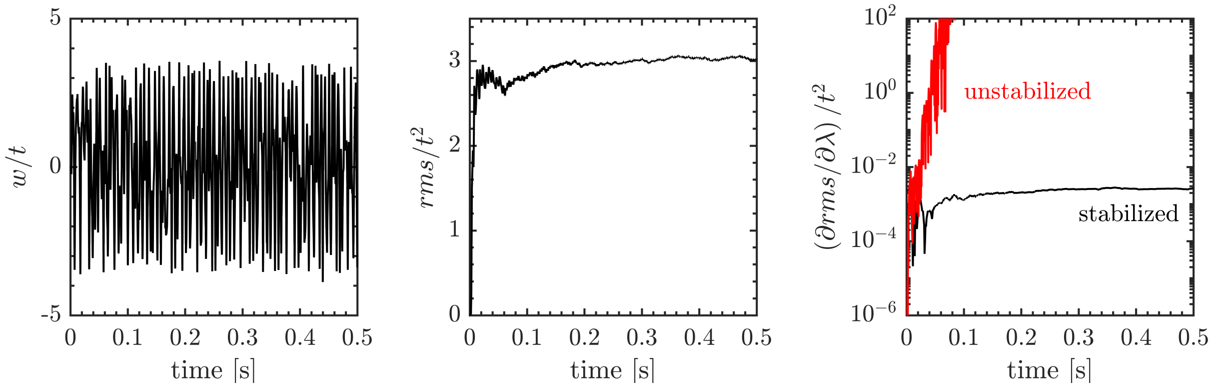

Figure 3: Panel response (left), RMS (center) and RMS derivatives with respect to λ (right), at $R/R_{cr} = 10$, $\lambda = 600$.

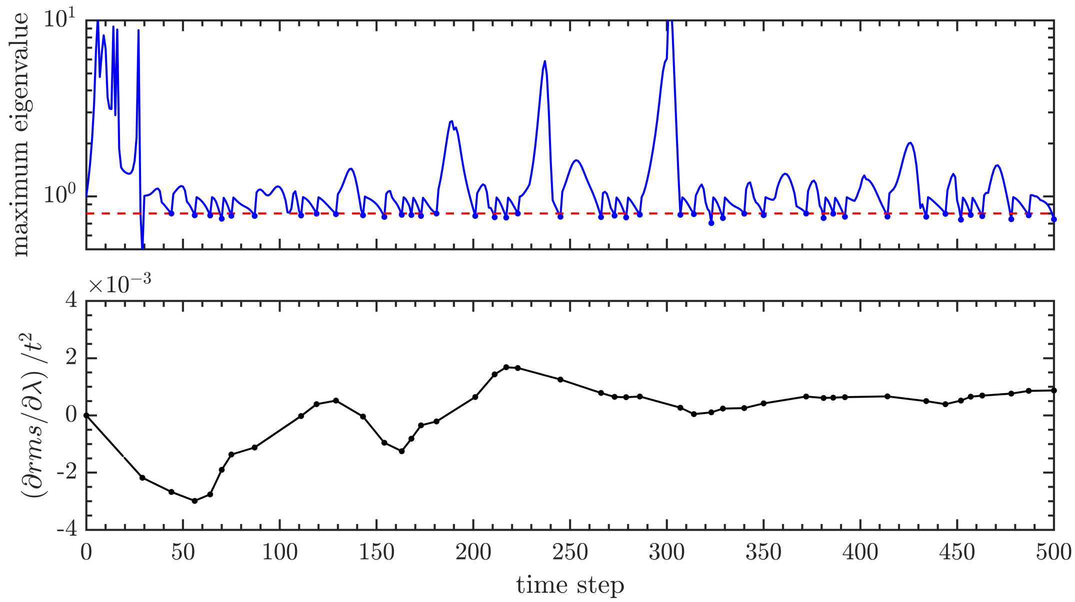

Figure 4: Demonstration of the adaptive time stepping stabilization procedure for the first 0.05 seconds of Fig. 3, with a limiting a value of 0.8.

(across the 100 simulations) are present at a given value of λ, reflected by the error bars. An estimation of the derivative is computed by finite-differencing each combination of data points across consecutive λ values, and the range of sensitivity estimations is shown by the gray shaded region on the right of Fig. 5. This is compared to analytical computations from the stabilization procedure, across a range of limiting eigenvalue thresholds (a) from 0.7 to 1.0. A value of 1.0 provides both an innacurate result, as well as large variations in the sensitivity from one simulation to the next. For this case, values of 0.8 and 0.9 provide the best result, and the optimal choice of a is, in general, ad-hoc.

B. Optimization Results

As noted above, the optimization problem solved here finds the smallest deviation in the structural thickness distribution (from the baseline, uniform, distribution) which will set the RMS of the output to some specified value. The design variables are the thickness of each finite element, which may range from 0.4 to 4.0 times the baseline value. Because there are a large number of design variables, adjoint reverse-time versions of the stabilized time marching schemes (Eq. 5) must be used, and their derivation can be found in Refs. 6 and 7. If $\boldsymbol{t}_{DV}$ is the vector of thickness design variables, and t_0 is the baseline thickness, then the objective function to

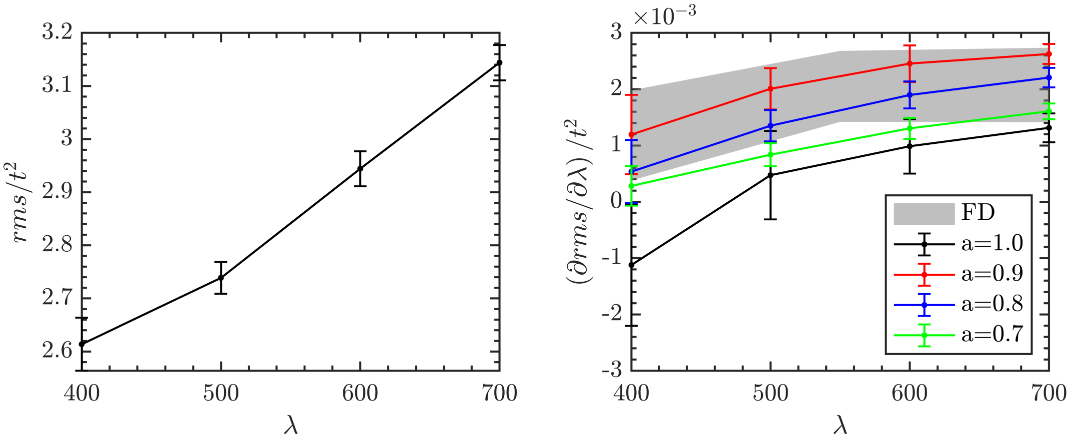

Figure 5: Verification of RMS sensitivities with respect to λ, comparing finite difference estimations (FD) against analytical computations.

be minimized is $\|\boldsymbol{t}_{DV} - t_0\|$. A single equality constraint is placed on the RMS motion at the three-quarters chord location. This optimization problem is solved with the Method of Moving Asymptotes.[9]

It is unclear, a-priori, which strategies the optimizer will take to drive the RMS motion to a certain limit, with the smallest possible deviation in the thickness distribution. If the RMS is to be decreased below a nominal baseline value, the optimizer cannot simply increase the panel thickness to stiffen the structure, because higher thicknesses will also increase the compressive forces seen by the panel, as the stresses (via the R term in Fig. 2) are prescribed. As will be seen below, more complex material distribution strategies are required, and thus a good candidate for gradient-based optimization.

Optimization results are shown in Fig. 6 for R/R_{cr} set to 10 and λ set to 600. The gradient-based optimization process is repeated several times across a range of RMS constraints, to map out the optimal trade-off curve (Pareto front) between the constraint and the thickness deviation objective function. The nonlinear dynamics of the optimal panel structure could be chaotic or LCO, and this is indicated in the figure. The plotted error bars, for both the objective function and the RMS constraint, indicate the variation in these metrics across the final 15 iterations of the optimization process. In general for gradient based optimization, one would expect a strong convergence to the optimal solution, but given the fluctuations previously noted in the gradient computations (Fig. 5), a strong convergence is not typically noted for chaotic dynamics. For LCO responses, the optimization fluctuations are much smaller, given the relative ease with which LCO-based gradients can be computed.

The baseline design in Fig. 6 occurs nearly at an RMS value of 3, which corresponds to a uniform-thickness design, and whose results are previously seen in Fig. 3. Given that the $\boldsymbol{t}_{DV}$ vector is entirely equal to t_0 here, the objective function $\|\boldsymbol{t}_{DV} - t_0\|$ is 0. Moving the RMS constraint to a value higher or lower than 3 forces a penalty in the objective function also. The optimizer is able to force the RMS up to 3.75, after which discontinuities appear in the design space which preclude further optimization, as will be discussed below. In the other direction, the optimizer is able to force the RMS to nearly 0.15, though for RMS constraints between 1 and 2.5, the response is a cleaner LCO; below an RMS of 1, the response again becomes chaotic. A fold in the Pareto front is also seen between RMS values of 1 and 1.5, where a decrease in the RMS constraint (i.e., a constraint which is harder to satisfy) actually leads to an improvement in the objective function, rather than a penalty.

Further results are shown in Fig. 7 for the optimal designs at RMS constraint thresholds of 0.15, 1.50, 2.00, 3.00, and 3.75. The top row of this figure shows the response history of each optimal design, the middle row shows the optimization convergence history, and the bottom row shows the final optimal thickness distribution. As above, results are only shown through 0.5 seconds, but simluations in actuality are integrated through 10 seconds. Echoing the results shown in Fig. 6, Fig. 7 shows a chaotic low-amplitude result at the 0.15-RMS value, with a relatively disjointed convergence history, particularly in the first 20 iterations. The LCO results (RMS values of 1.50 and 2.00) show a strong and rapid convergence to the optima (indicated by the small error bars in Fig. 6 also); the 1.50-RMS result, which is the top of the Pareto fold, shows a multi-harmonic LCO, whereas the 2.00-RMS result is a simpler single-harmonic LCO. An RMS constraint

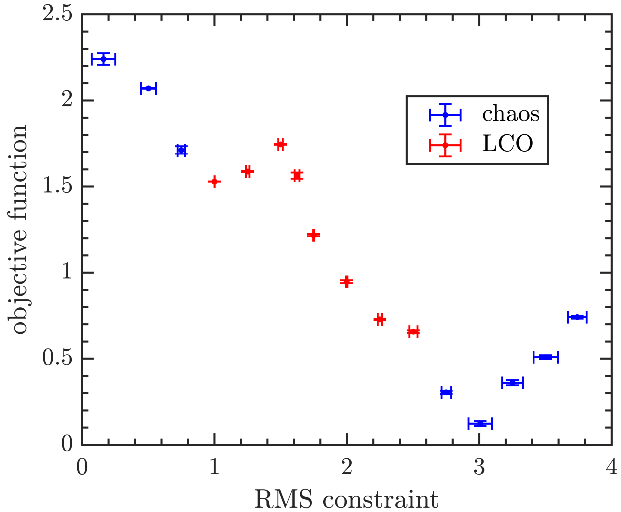

Figure 6: Optimal trade-off curve between the prescribed RMS motion of the fluttering panel (constraint), and the thickness deviation (objective function).

value of 2.50 is the highest-RMS optima with an LCO response, and this optimal time history transitions from chaos to LCO mid-simulation, as seen in Fig. 8

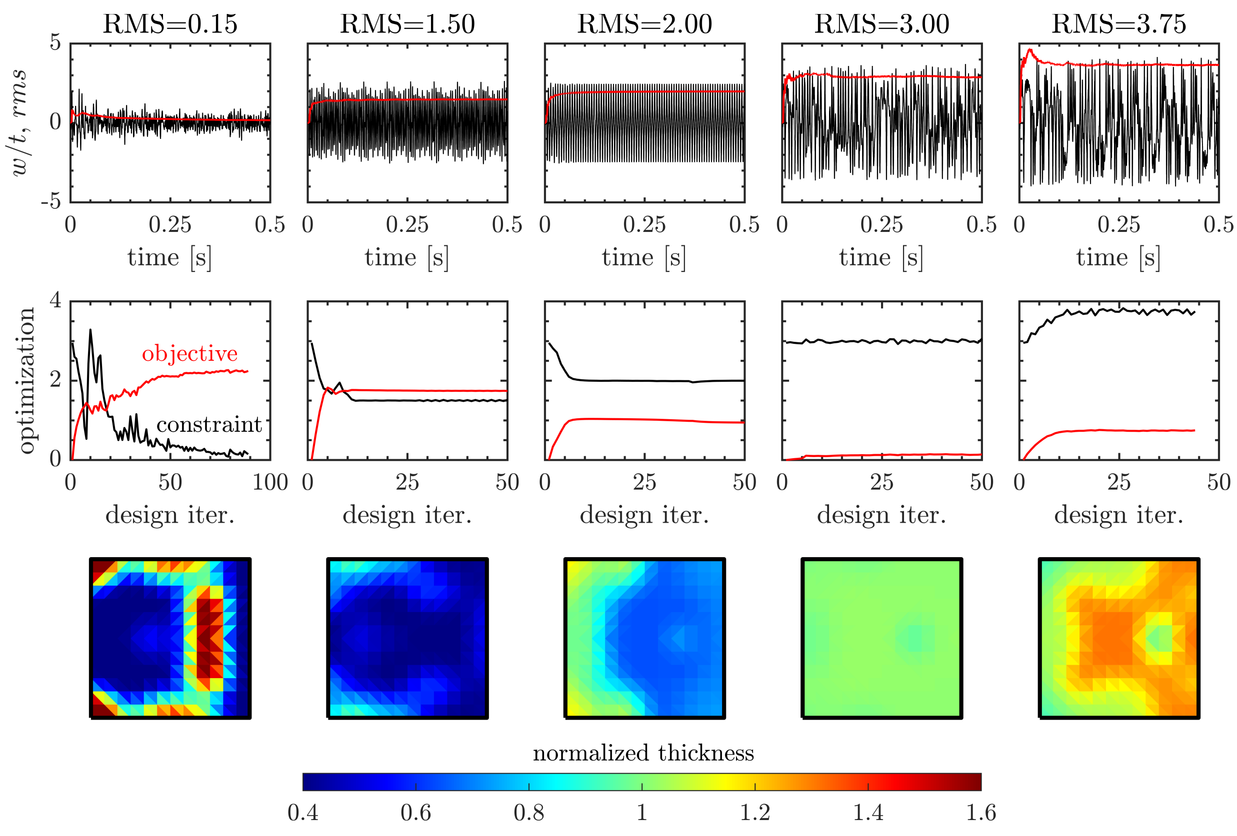

Figure 7: Optimal results at RMS constraint thresholds of 0.15, 1.50, 2.00, 3.00, and 3.75: optimal response dynamics (top row), optimization convergence (middle row), optimal thickness distribution (bottom row).

The final two results in Fig. 7 are chaotic results with RMS values of 3.00 and 3.75, and these optimal convergence histories display the fluctuations also indicated in the error bars of Fig. 6. The limiting a value for eigenvalue stabilization is set to 0.8 here; a smaller value will lead to more damping in the sensitivities,

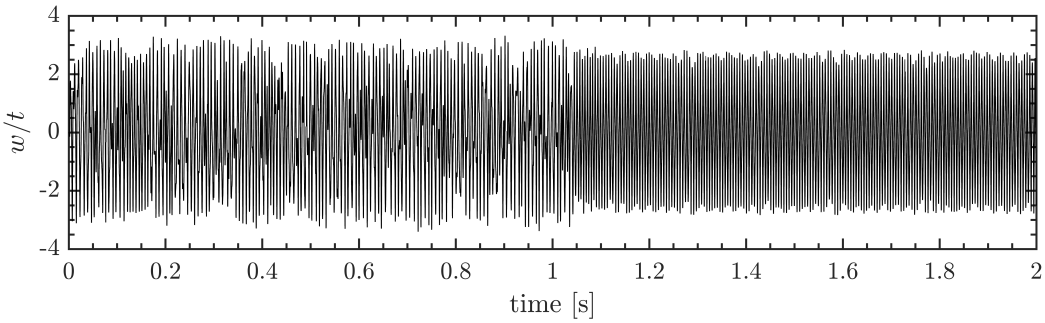

Figure 8: Optimal response history at an RMS constraint threshold of 2.50.

likely slower optimization convergence but perhaps weaker fluctuations as well, though this has not been explored here. These high-RMS optimal chaotic thickness distributions are characterized by thick structures along the trailing edge and near the mid-point of the panel; the three-quarters chord point (where the RMS constraints are measured) shows relatively low thickness. The thickness trends for the low-RMS designs is nearly opposite each of those spatial trends.

As noted previously, for RMS constraints set at or above 4.0, the design space becomes discontinuous, and the gradient-based optimization fails. This is shown in Fig. 9, when the RMS constraint threshold is set to 4.00. At design iteration 19 (nearly equal to the constraint boundary of 4.00), a chaotic response is shown, but one with an intermittent and temporary attraction to a statically-buckled solution. At the next iteration (20) the design has statically-buckled, and then returns to a chaotic solution at iteration 21 again.

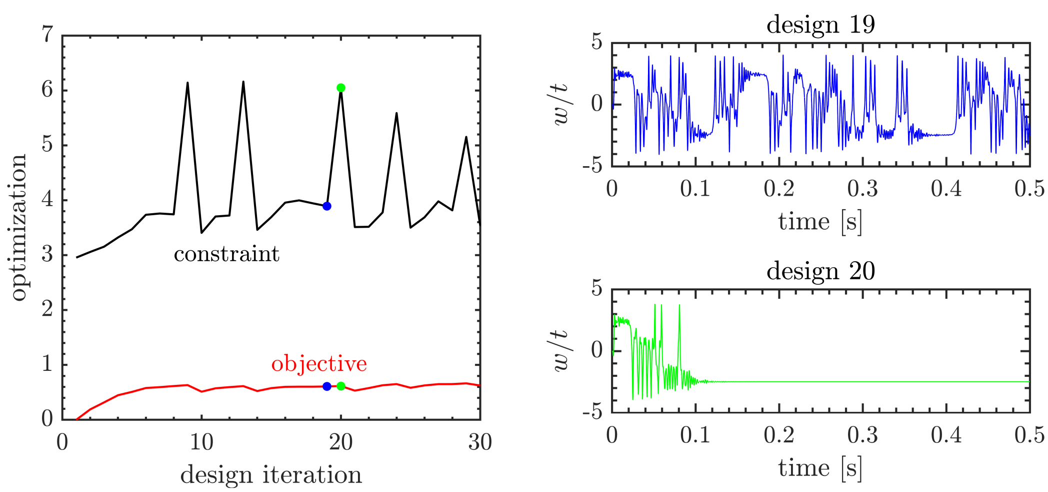

Figure 9: Discontinuities in the optimal response history at an RMS constraint threshold of 4.00.

IV. Conclusions

This work has presented an extension of Refs. 6 and 7 , where the stabilized sensitivity analysis presented in those papers has been extended to the chaotic aeroelastic flutter of a two-dimensional panel. First, the accuracy of panel vibration RMS derivatives with respect to a dynamic pressure parameter has been verified, using a direct method. Next, adjoint derivatives with respect to the local skin thickness values have been utilized in a gradient-based optimization demonstration, where it is desired to force the RMS of the panel vibration to a certain level (equality design constraint) in a way that minimizes deviations from the baseline thickness distribution (objective function).

High-RMS designs are characterized by chaotic dynamics and fluctuations in the optimization history, which can be traced to nondeterministic aspects of the gradient computation procedure. Setting the RMS threshold too high above the baseline value leads to discontinuities in the response, which alternates between static buckling and chaotic dynamics, and the optimization fails. Low-RMS designs see a switch from chaos to cleaner LCO outputs, and stronger convergence of the optimization procedure. Decreasing the RMS threshold to very-low values leads to a transition back to chaos, however.

Acknowledgments

In memory of Prof. Manav Bhatia, a great friend and intellect.

References

[1]Dowell, E., "Flutter of a Buckled Plate as an Example of Chaotic Motion of a Deterministic Autonomous System" *Journal of Sound and Vibration*, Vol. 85, No. 3, pp. 333-344, 1982.

[2]Wang, Q., Hu, R., Blonigan, P., "Least Square Shadowing Sensitivity Analysis of Chaotic Limit Cycle Oscillations" *Journal of Computational Physics*, Vol. 267, pp. 210-224, 2014.

[3]Blonigan, P., Wang, Q., "Multiple Shooting Shadowing for Sensitivities Analysis of Chaotic Dynamical Systems" *Journal of Computational Physics*, Vol. 354, pp. 447-475, 2018.

[4]Karbasian, H., Vermeire, B., "Sensitivity Analysis of Chaotic Dynamic Systems using a Physics-Constrained Data-Driven Approach" *Physics of Fluids*, Vol. 34, No. 014101, 2022.

[5]Donello, M., Carpenter, M., Babaee, H., "Computing Sensitivities in Evolutionary Systems: a Real-Time Reduced Order Modeling Strategy" *SIAM Journal on Scientific Computing*, Vol. 44, No. 1, pp. 1-12, 2022.

[6]Bhatia, M., Makhija, D., "Sensitivity Analysis of Time-Averaged Quantities of Chaotic Systems" *AIAA Journal*, Vol. 57, No. 5, pp. 2088-2099, 2019.

[7]Bhatia, M., Taoudi, L., "Assessment of Stabilized Sensitivity Solution Approach for High-Dimensional Chaotic Systems" *AIAA SciTech Forum*, San Diego, CA, Jan. 7-11, 2019.

[8]Mei, C., Abdel-Motagaly, K., Chen, R., "Review of Nonlinear Panel Flutter at Supersonic and Hypersonic Speeds" *Applied Mechanics Reviews*, Vol. 52, No. 10, pp. 321-331, 1999.

[9]Svanberg, K., "The Method of Moving Asymptotes - a New Method for Structural Optimization," *International Journal for Numerical Methods in Engineering*, Vol. 24, No. 2, pp. 359-373, 1987.